encit 2020

ABCM
Associação Brasileira de Engenharia e Ciências Mecânicas

18th Brazilian Congress of Thermal Sciences and Engineering
November 16–20, 2020 (Online)

ENC-2020-0165
A Two-Dimensional Element-Based Finite Volume Method for Solving the Poroelastic Problem

Gustavo G. Ribeiro
Fernando S. V. Hurtado
Engineering Simulation and Scientific Software (ESSS)
ggrbill@gmail.com
ferveh@gmail.com

Clovis R. Maliska
Computational Fluid Dynamics Laboratory (SINMEC), Mechanical Engineering Departament (EMC), Federal University of Santa Catarina (UFSC)
maliska@sinmec.ufsc.br

Abstract. *The present work considers the Biot's theory of consolidation for deriving a numerical model for solving coupled fluid flow and geomechanics problems in porous media. Normally these equations are solved using different numerical tools, being the most common approach the use of the finite element method for the geomechanical problem and the finite volume method for the fluid flow problem. The use of finite element for the rock mechanics is mainly a tradition of using this method for solid mechanics.In this work, in the other hand, both problems are solved using a finite volume technique, the Element-based Finite Volume Method (EbFVM), in the framework of the same two-dimensional unstructured grid. The coupled system of discretized equations is solved in an iterative way, in which the equation of each model are solved separately, exchanging information at all time steps. Two classic problems with known analytical solutions are solved to validate the proposed numerical approach, the Terzaghi's poroelastic column and mandel's problem. In both cases the obtained numerical solutions are very close to the analytical ones, showing that the presented methodology is very promising for solving coupled problems.*

Keywords: *geomechanics, poroelastic problem, finite volume method, unstructured grids, coupled solution*

1. INTRODUCTION

In Terzaghi (1923) the one-dimensional consolidation problem, known as Terzaghi's column was used to introduce the effective stress concept. After that, Biot (1941) developed the three-dimensional theory of consolidation, generalizing Terzaghi's consolidation theory. Besides that, he went further in this theory expanding it for anisotropic and non-linear materials (Biot, 1955, 1956). In 1966, Geertsma (1966) used for the first time the term poroelasticity to refer to this theory. He pointed out that Biot's consolidation theory was developed to describe elastic and viscoelastic rock materials saturated with some fluid, and its mathematical description is similar to the termoelasticity theory. Later, Rice and Cleary (1976) rewrote the same theory on the basis of new mensurable poroelastic properties. Detournay and Cheng (1993) discussed the separated treatment of the fluid and solid phases, formalizing the theory in terms of the constituent phases properties, which is more convenient. This new treatment was possible because the authors introduced the concept of drained and undrained conditions of the porous medium.

Usually, obtaining analytical solutions for physical problems is a very difficult task, unless some especial conditions are considered. The geomechanical problems are not different and just for a few cases it is possible to obtain an analytical solution. Terzaghi's one-dimensional consolidation problem (Terzaghi, 1923), Mandel's two-dimensional problem (Mandel, 1953) and Cryer's sphere (Cryer, 1963) are examples of this kind of problems. Therefore, the numerical solution is the only feasible alternative to obtain a solution of practical consolidation problems.

The poroelasticity models two different kind of problems, fluid flow and geomechanics, which together describe the mechanical compaction of a porous rock. The fluid flow in porous media is usually solved numerically by the finite volume method (FVM) (Peaceman, 1977; Aziz and Settari, 1979) because it is conservative in the discrete level. This feature is very important when transport phenomena are being solved numerically, otherwise it would be possible to obtain results with mass source or sink which are not physically accepted. On the other hand, the geomechanics is usually solved applying finite element methods (FEM) (Zienkiewicz and Taylor, 2000) by the tradition in solving solid mechanics problems with this method. In petroleum reservoir simulation it is common to use FEM to solve the geomechanics

problem (Raghavan *et al.*, 1972; Gutierrez and Lewis, 1998; Chin *et al.*, 2000; Chen *et al.*, 2006), while FVM is used for the fluid flow in the reservoir (Peaceman, 1977; Aziz and Settari, 1979; Mattax and Dalton, 1990).

The first efforts to solve the coupled compaction problem in engineering level were made by coupling commercial reservoir simulators with FEM algorithms (Settari and Walters, 2001; Tran *et al.*, 2004; Li *et al.*, 2006; Benisch *et al.*, 2020). However, the difference between FVM and FEM grids adds an interpolation issue, once the location of the discrete variables is not the same. In order to eliminate the necessity of interpolation between discrete values of different grids (Chin *et al.*, 2002) and (Thomas *et al.*, 2002, 2003) developed an algorithm that simulates the fluid flow with finite differences method (FDM) and the porous rock compaction with FEM in the same cartesian grid. Following this kind of approach, Gutierrez and Lewis (2002) employed FEM to solve both the fluid flow and the geomechanics equations. Some works followed that approach (Ferronato *et al.*, 2010; Mikelič *et al.*, 2014), but using a mixed finite element method (MFEM) (Klausen and Russel, 2004) to solve the fluid flow through the porous rock, what adds some additional computational costs. Possibly that choice was made because FEM is not conservative in the discrete level bringing up problems in the solution of the fluid flow. As mentioned before, this feature is very important to solve numerically fluid flow problems.

In the context of finite volume methods some works as Shaw and Stone (2005), Dal Pizzol and Maliska (2012), among others, progressed in order to solve both problems using FVM. In the first work mentioned, Shaw and Stone (2005) developed a general finite volume discretization that can be plugged into an existent reservoir simulator. Dal Pizzol and Maliska (2012), in the other hand, developed a coupled formulation using a staggered arrangement of variables and a finite volume method for both physics. In this arrangement, the displacements and pressure discrete values are placed in a way that interpolation is not necessary at all.

Following the trend of solving both the fluid flow and the geomechanics problems with a single methodology in a single grid, a strategy that employs a finite volume method able to deal with two-dimensional unstructured grids is developed in this work. The main concern was to guarantee that all conservation laws are satisfied identically in the discrete level. In addition to that, using an unstructured grid turns the method more flexible in cases with complex geometries. The Element-based finite volume method (EbFVM) is the methodology used to discretize the poroelasticity differential equations in this work. This method possesses all those features and was successfully applied to the solution of both fluid flow (Rozon, 1989; Forsyth, 1990; Gottardi and Dall'olio, 1992) and mechanical behavior (Filippini *et al.*, 2014) separately. The iterative solution strategy used is the two-way coupling which both problems are solved iteratively in each time step. Obviously, when the convergence is reached, the solution is the same as if all equations were solved simultaneously (Settari and Walters, 2001).

2. Mathematical model

The porous medium compaction is described by Biot's theory of consolidation which connects two physical phenomena, the fluid flow and the geomechanics. The fluid flow through the porous media is a well-known phenomenon described by Darcy's law. On the other hand, the mechanical behavior of the medium is represented as a force balance equation in which the Terzaghi's effective stress concept is applied. The complete model of the phenomenon is described by the combination between those equations. In addition, the coupling is given by the presence of pressure into force balance equation and the presence of volumetric strain into mass conservation equation.

2.1 Geomechanics equations

The geomechanical behavior can be described as a force balance equation, given by

$$\boldsymbol{\nabla} \cdot \left(\bar{\boldsymbol{\sigma}} - \alpha P \bar{\mathbf{I}} \right) = 0 \,, \tag{1}$$

in which $\boldsymbol{\nabla}$ is the nabla operator, $\bar{\boldsymbol{\sigma}}$ is the Terzaghi's effective stress tensor acting on the porous matrix, P is the fluid pore pressure, $\bar{\mathbf{I}}$ is the identity tensor and α is the Biot's coefficient. The effective stress is related to the total stress through

$$\bar{\boldsymbol{\sigma}} = \bar{\boldsymbol{\sigma}}_{tot} + \alpha P \bar{\mathbf{I}} \,, \tag{2}$$

where $\bar{\boldsymbol{\sigma}}_{tot}$ is the total stress tensor. It is important to note that the Biot's coefficient is a physical property of the porous rock and represents which parcel of the pressure enters for supporting the total stress applied on the rock structure. (Wang, 2000).

The constitutive equation for the effective stress is defined by Hooke's law, given by

$$\bar{\boldsymbol{\sigma}} = \bar{\mathscr{D}} : \bar{\boldsymbol{\varepsilon}} \,, \tag{3}$$

in which $\bar{\mathscr{D}}$ is the constitutive fourth-order tensor and $\bar{\boldsymbol{\varepsilon}}$, the strain tensor, is defined by

$$\bar{\boldsymbol{\varepsilon}} = \frac{\boldsymbol{\nabla}\mathbf{u} + (\boldsymbol{\nabla}\mathbf{u})^T}{2} \,, \tag{4}$$

in which $\mathbf{u}$ is the displacement vector, whose components are u and v.

Assuming an isotropic elastic material, Eq. (3) becomes

$$\bar{\boldsymbol{\sigma}} \;=\; 2G\bar{\boldsymbol{\varepsilon}} + \lambda\,\mathsf{tr}(\bar{\boldsymbol{\varepsilon}})\,\bar{\mathbf{I}}\,, \tag{5}$$

in which G and λ are Lamé's parameters and $\mathsf{tr}(\,\cdot\,)$ is the trace operator. Substituting Eq. (5) and Eq. (4), in Eq. (1), it is obtained an equation with two variables, $\mathbf{u}$, the displacement vector, and P, the fluid pore pressure.

2.2 Fluid flow equations

For closing the model, it is introduced the fluid mass conservation for a deformable porous medium, given by

$$(\phi c_f(\alpha-\phi)c_s)\,\frac{\partial P}{\partial t} + \boldsymbol{\nabla}\cdot\mathbf{v} \;=\; f - \alpha\frac{\partial \varepsilon_v}{\partial t}\,, \tag{6}$$

in which c_f is the fluid compressibility, c_s the solid grain compressibility, ϕ the porosity, ε_v the volumetric strain defined by

$$\varepsilon_v \;=\; \mathsf{tr}(\bar{\boldsymbol{\varepsilon}}) \tag{7}$$

and $\mathbf{v}$ is the Darcy's velocity defined by

$$\mathbf{v} \;=\; -\frac{1}{\mu}\bar{\mathbf{K}}\boldsymbol{\nabla}P\,, \tag{8}$$

where μ is the fluid viscosity and $\bar{\mathbf{K}}$ is the absolute permeability of the rock.

It is important to note that this model considers a slightly compressible fluid (Peaceman, 1977). As can be observed, the mathematical model is closed, since there are two equations, Eq. (1) and Eq. (6), and two unknowns, the fluid pore pressure and the porous matrix displacement vector.

3. Numerical model

As explained before, both fluid flow and geomechanics are solved herein by only one numerical method, the Element-based Finite Volume Method (EbFVM). This methodology is a finite volume method able to deal with unstructured grids presented initially by Baliga and Patankar (1980, 1983) under the name of Control Volume Finite-Element Method (CVFEM).

3.1 Element based Finite Volume Method

The first step in devising a numerical method is the discretization of the domain, that is, its subdivision in much smaller sub-domains. In EbFVM, those sub-domains are called elements and have a simple geometric shape. In this work triangular and quadrangular elements are used. The elements are used to construct the control volumes as well as for locating the physical properties of the porous medium. Another fundamental entity is the node, located at the element corners and where all unknowns of the problem are approximated. As can be seen in Fig. 1(a), a control volume is built around each node and is formed by portions of the elements sharing that node. The control surface that delimits the control volume is composed by a certain number of faces. A face is an entity obtained connecting a midpoint of an element side to the center of the element.

Any face links two control volumes, or in other words, any face is shared by two neighboring control volumes. Figure 1(b) shows an arbitrary face f that is shared by two control volumes associated to nodes nF and nB. Those nodes will be named forward node and backward node, respectively, relative the face area vector $\Delta\mathbf{S}_\mathsf{f}$. The face area vector is a vector which its magnitude is the value of area of the face and it is perpendicular to the face. Each face has a face area vector $\Delta\mathbf{S}_\mathsf{f}$ with a unique orientation.

The EbFVM, as any finite volume method, generate the approximated equations, through a balance of the property at the control volume, or integrating the conservation equations in a conservative form in space and time. In any case all calculations are performed at element level, and the approximate equations for every control volume are assembled summing up the contributions coming from all surrounding elements. For quadrangular and triangular elements the coordinate transformation can be conveniently expressed using shape functions. Bilinear shape functions are usually used for quadrilateral, as

$$\begin{cases} N_1(\xi,\eta) \;=\; \frac{1}{4}(1+\xi)(1+\eta)\,, \\ N_2(\xi,\eta) \;=\; \frac{1}{4}(1-\xi)(1+\eta)\,, \\ N_3(\xi,\eta) \;=\; \frac{1}{4}(1-\xi)(1-\eta)\,, \\ N_4(\xi,\eta) \;=\; \frac{1}{4}(1+\xi)(1-\eta)\,, \end{cases} \tag{9}$$

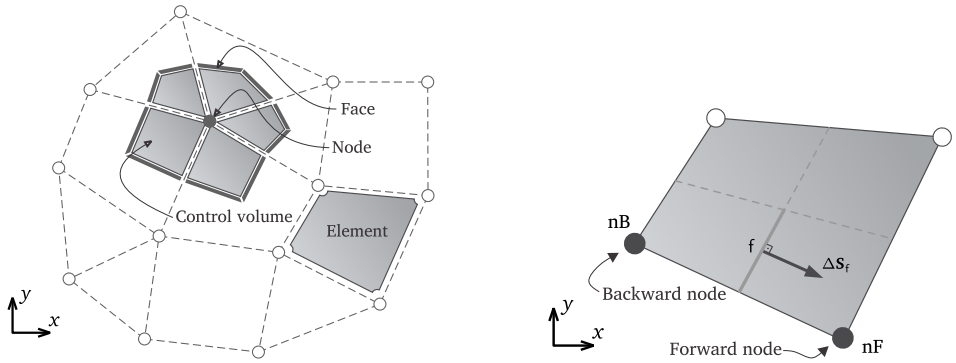

(a) Main geometric entities. (b) Face f and its backward and forward nodes.

Figure 1. EbFVM geometrical properties.

whereas linear shape functions suffices for triangular elements, as

$$\begin{cases} N_1(\xi,\eta) \;=\; 1-\xi-\eta\,, \\ N_2(\xi,\eta) \;=\; \xi\,, \\ N_3(\xi,\eta) \;=\; \eta\,. \end{cases} \tag{10}$$

The local coordinates (ξ,η) are related to the global coordinate system by the transformation equations

$$\begin{cases} x(\xi,\eta) \;=\; \displaystyle\sum_{\mathsf{p}\in\mathscr{N}^{\mathsf{e}}} N_{\mathsf{p}}(\xi,\eta)x_{\mathsf{p}}\,, \\ y(\xi,\eta) \;=\; \displaystyle\sum_{\mathsf{p}\in\mathscr{N}^{\mathsf{e}}} N_{\mathsf{p}}(\xi,\eta)y_{\mathsf{p}}\,, \end{cases} \tag{11}$$

in which x_{p} and y_{p} are the global coordinates of each node $\mathsf{p}\in\mathscr{N}^{\mathsf{e}}$, being $\mathscr{N}^{\mathsf{e}}$ the set of nodes located at vertices of an arbitrary element e. An important fact is that no matter how distorted an element is in terms of global coordinates, it will became always a regular triangle or square in the transformed plane (Zienkiewicz and Taylor, 2000).

In order to calculate the value of any variable Θ, inside the element, an analogous expression to Eq. (11) is considered, as

$$\Theta(\xi,\eta) \;=\; \sum_{\mathsf{p}\in\mathscr{N}^{\mathsf{e}}} N_{\mathsf{p}}(\xi,\eta)\Theta_{\mathsf{p}}\,, \tag{12}$$

in which Θ_{p} are the discrete value associated to each element node. Employing this approximation, it is easy to find the gradient of Θ differentiating Eq. (12), giving

$$\boldsymbol{\nabla}\Theta \;=\; (\mathbf{J}^{\mathsf{e}})^{-\mathrm{T}}(\mathbf{D}^{\mathsf{e}})^{\mathrm{T}}\boldsymbol{\Theta}^{\mathsf{e}}\,, \tag{13}$$

where $\boldsymbol{\Theta}^{\mathsf{e}}$ is a column vector containing the discrete values of variable Θ at the nodes of element e. Additionally, $\mathbf{D}^{\mathsf{e}}$ is an auxiliary matrix that contains the partial derivatives of shape functions and $N_{\mathrm{n}}(\mathsf{e})$ is the number of nodes on element e, 3 for a triangular element and 4 for a quadrangular element. The Jacobian matrix $\mathbf{J}^{\mathsf{e}}$ of the coordinate transformation can be obtained from the matrix product

$$\mathbf{J}^{\mathsf{e}} \;=\; \mathbf{X}^{\mathsf{e}}\mathbf{D}^{\mathsf{e}} \;=\; \begin{pmatrix} x_1 & x_2 & \cdots & x_{N_{\mathrm{n}}(\mathsf{e})} \\ y_1 & y_2 & \cdots & y_{N_{\mathrm{n}}(\mathsf{e})} \end{pmatrix} \begin{pmatrix} \partial_\xi N_1 & \partial_\eta N_1 \\ \partial_\xi N_2 & \partial_\eta N_2 \\ \vdots & \vdots \\ \partial_\xi N_{N_{\mathrm{n}}(\mathsf{e})} & \partial_\eta N_{N_{\mathrm{n}}(\mathsf{e})} \end{pmatrix}, \tag{14}$$

where the entries of matrix $\mathbf{X}^{\mathsf{e}}$ are the global coordinates of the nodes in the element e. Further geometric details of the discretization process can be found in Raw (1985).

3.2 Discretization

As mentioned in section 2.in this work it is considered a single-phase fluid flow through deformable porous medium. This section is devoted to show the discretization of Eq. (1) and Eq. (6), applying EbFVM.

The final form of the fluid flow mass conservation equation is obtained substituting Eq. (8) in Eq. (6), giving

$$(\phi c_f(\alpha-\phi)c_s)\,\frac{\partial P}{\partial t} - \boldsymbol{\nabla}\cdot\left(\frac{1}{\mu}\bar{\mathbf{K}}\boldsymbol{\nabla}P\right) \;=\; -\alpha\frac{\partial \varepsilon_v}{\partial t}\,, \tag{15}$$

in which the main unknown is the fluid pore pressure P. In fact, according to the coupling strategy used, only pressure P is considered an active variable in this equation. This means that the volumetric strain, ε_v, comes from the geomechanics problem as a known variable. Consequently, the third term on Eq. (15) is a source term whose value is already known.

The discretization applying EbFVM starts with the volumetric and temporal integration of every term of a differential equation in a generic control volume. Thus, for Eq. (15), it is obtained

$$[\phi_{\mathsf{p}} c_f + (\alpha - \phi_{\mathsf{p}}) c_s] \, \Delta V_{\mathsf{p}} P_{\mathsf{p}} - \frac{\Delta t}{\mu} \sum_{\mathsf{e} \in \mathscr{E}_{\mathsf{p}}} \sum_{\mathsf{f} \in \mathscr{F}_{\mathsf{p}}^{\mathsf{e}}} (\boldsymbol{\beta}_{\mathsf{f}}^{\mathsf{e}})^{\mathrm{T}} \, \mathbf{P}^{\mathsf{e}} \;=\; [\phi_{\mathsf{p}} c_f + (\alpha - \phi_{\mathsf{p}}) c_s] \, \Delta V_{\mathsf{p}} P_{\mathsf{p}}^{o} - \alpha \left(\varepsilon_{v,\mathsf{p}} - \varepsilon_{v,\mathsf{p}}^{o} \right) \Delta V_{\mathsf{p}} \,, \tag{16}$$

in which Δt is the time step, ΔV_{p} is the volume of the control volume associated to a generic node p, P_{p} is the discrete pressure associated to the same node and P_{p}^{o} is the same pressure at the previous time level. The discrete form of the flux term includes $\boldsymbol{\beta}_{\mathsf{f}}^{\mathsf{e}}$, which is a vector operator associated to a generic face f inside of an element e, defined by

$$(\boldsymbol{\beta}_{\mathsf{f}}^{\mathsf{e}})^{\mathrm{T}} \;=\; \Delta \mathbf{S}_{\mathsf{f}}^{\mathrm{T}} \mathbf{K}^{\mathsf{e}} \mathbf{J}_{\mathsf{f}}^{-\mathrm{T}} \mathbf{D}_{\mathsf{f}}^{\mathsf{e},\mathrm{T}} \,, \tag{17}$$

where $\mathbf{K}^{\mathsf{e}}$ is the permeability tensor associated to the element e. It is important to note that the flux term in (16) involves two summations, one over the elements and one over the faces inside the elements.

Also $\varepsilon_{v,\mathsf{p}}$ and $\varepsilon_{v,\mathsf{p}}^{o}$ are the discrete volumetric strain in the current and previous time level, associated to the control volume p, respectively. Those values come from the geomechanics problem and are considered already known when solving the mass conservation equation, as previously mentioned.

When Eq. (16) is written for all control volumes on the grid, we obtain the linear system

$$\mathbf{A}\mathbf{P} \;=\; \mathbf{b} \,, \tag{18}$$

in which $\mathbf{A}$ is the coefficient matrix, $\mathbf{b}$ is the independent vector and $\mathbf{P}$ is the vector whose components are the discrete pressure values associated to all control volumes of the grid.

Since Eq. (1) is a vector equation, the more simple way of discretizing it is to treat its components in each Cartesian direction separately. Therefore, we can write

$$\sum_{\mathsf{e} \in \mathscr{E}_{\mathsf{p}}} \sum_{\mathsf{f} \in \mathscr{F}_{\mathsf{p}}^{\mathsf{e}}} (\boldsymbol{\Gamma}_{x,\mathsf{f}}^{\mathsf{e}})^{\mathrm{T}} \, \mathbf{u}^{\mathsf{e}} + \sum_{\mathsf{e} \in \mathscr{E}_{\mathsf{p}}} \sum_{\mathsf{f} \in \mathscr{F}_{\mathsf{p}}^{\mathsf{e}}} (\boldsymbol{\Lambda}_{x,\mathsf{f}}^{\mathsf{e}})^{\mathrm{T}} \, \mathbf{v}^{\mathsf{e}} \;=\; \alpha (\partial_x P)_{\mathsf{p}} \Delta V_{\mathsf{p}} \tag{19}$$

$$\sum_{\mathsf{e} \in \mathscr{E}_{\mathsf{p}}} \sum_{\mathsf{f} \in \mathscr{F}_{\mathsf{p}}^{\mathsf{e}}} (\boldsymbol{\Lambda}_{y,\mathsf{f}}^{\mathsf{e}})^{\mathrm{T}} \, \mathbf{u}^{\mathsf{e}} + \sum_{\mathsf{e} \in \mathscr{E}_{\mathsf{p}}} \sum_{\mathsf{f} \in \mathscr{F}_{\mathsf{p}}^{\mathsf{e}}} (\boldsymbol{\Gamma}_{y,\mathsf{f}}^{\mathsf{e}})^{\mathrm{T}} \, \mathbf{v}^{\mathsf{e}} \;=\; \alpha (\partial_y P)_{\mathsf{p}} \Delta V_{\mathsf{p}} \,, \tag{20}$$

in which Eq. (19) and Eq. (20) are the discrete balance force equations related to each Cartesian directions. The discrete operators are given by

$$\begin{aligned}
(\boldsymbol{\Gamma}_{x,\mathsf{f}}^{\mathsf{e}})^{\mathrm{T}} &\;=\; \Delta \mathbf{S}_{\mathsf{f}}^{\mathrm{T}} \mathbf{K}_{uu}^{\mathsf{e}} \mathbf{J}_{\mathsf{f}}^{-\mathrm{T}} \mathbf{D}_{\mathsf{f}}^{\mathsf{e},\mathrm{T}} \,, \\
(\boldsymbol{\Gamma}_{y,\mathsf{f}}^{\mathsf{e}})^{\mathrm{T}} &\;=\; \Delta \mathbf{S}_{\mathsf{f}}^{\mathrm{T}} \mathbf{K}_{vv}^{\mathsf{e}} \mathbf{J}_{\mathsf{f}}^{-\mathrm{T}} \mathbf{D}_{\mathsf{f}}^{\mathsf{e},\mathrm{T}} \,, \\
(\boldsymbol{\Lambda}_{x,\mathsf{f}}^{\mathsf{e}})^{\mathrm{T}} &\;=\; \Delta \mathbf{S}_{\mathsf{f}}^{\mathrm{T}} \mathbf{P} \mathbf{K}_{uv}^{\mathsf{e}} \mathbf{J}_{\mathsf{f}}^{-\mathrm{T}} \mathbf{D}_{\mathsf{f}}^{\mathsf{e},\mathrm{T}} \,, \\
(\boldsymbol{\Lambda}_{y,\mathsf{f}}^{\mathsf{e}})^{\mathrm{T}} &\;=\; \Delta \mathbf{S}_{\mathsf{f}}^{\mathrm{T}} \mathbf{P} \mathbf{K}_{vu}^{\mathsf{e}} \mathbf{J}_{\mathsf{f}}^{-\mathrm{T}} \mathbf{D}_{\mathsf{f}}^{\mathsf{e},\mathrm{T}} \,.
\end{aligned} \tag{21}$$

As can be seen in Eq. (21), the discrete operators are similar to the discrete operator $\boldsymbol{\beta}_{\mathsf{f}}^{\mathsf{e}}$. The approach of using the same operator for discretized equations is very convenient, because it allows to use the same computational code responsible for computing all discrete operators. The only difference between them are the physical properties expressed by matrix $\mathbf{K}$.

The matrices are given by

$$\bar{\mathbf{K}}_{uu} \;=\; \begin{pmatrix} \frac{2G(1-\nu)}{(1-2\nu} & 0 \\ 0 & G \end{pmatrix} , \quad \bar{\mathbf{K}}_{vv} \;=\; \begin{pmatrix} G & 0 \\ 0 & \frac{2G(1-\nu)}{(1-2\nu)} \end{pmatrix} , \quad \bar{\mathbf{K}}_{uv} \;=\; \begin{pmatrix} G & 0 \\ 0 & \frac{2G\nu}{1-2\nu} \end{pmatrix} \text{and} \quad \bar{\mathbf{K}}_{vu} \;=\; \begin{pmatrix} \frac{2G\nu}{1-2\nu} & 0 \\ 0 & G \end{pmatrix} . \tag{22}$$

Finally, $\mathbf{P}$ is a permutation matrix with zeros on the diagonal and ones in the rest of the matrix values.

Equation (19) and Eq. (20) forms the coupled linear system for solving the displacements, given by

$$\begin{pmatrix} \mathbf{A}_u^x & \mathbf{A}_v^x \\ \mathbf{A}_u^y & \mathbf{A}_v^y \end{pmatrix} \begin{pmatrix} \mathbf{u}_h \\ \mathbf{v}_h \end{pmatrix} \;=\; \begin{pmatrix} \mathbf{b}_x \\ \mathbf{b}_y \end{pmatrix} , \tag{23}$$

where $\mathbf{u}_h$ and $\mathbf{v}_h$ are displacements vectors, whose components are the scalar displacements u and v for all node in the grid. The matrices $\mathbf{A}_u^x$, $\mathbf{A}_v^x$, $\mathbf{A}_u^y$ and $\mathbf{A}_v^y$ are formed by combinations of components of the discrete operators defined in

Eq. (21). The independent vectors $\mathbf{b}_x$ and $\mathbf{b}_y$ are formed by the right-hand side terms of Eq. (19) and Eq. (20), which is the discrete pore pressure term for each Cartesian direction.

In Eq. (16), Eq. (19) and Eq. (20), the source terms depend on the gradients $\boldsymbol{\nabla} u$, $\boldsymbol{\nabla} v$ and $\boldsymbol{\nabla} P$. Actually, the gradients of displacements, $\boldsymbol{\nabla} u$ and $\boldsymbol{\nabla} v$, are needed to compute the volumetric strain ε_{p}. Herein, those gradients are approximated by mean of the Green-Gauss formula (Blazek, 2001), as

$$(\boldsymbol{\nabla}\Theta)_{\mathsf{p}} \;=\; \frac{1}{\Delta V_{\mathsf{p}}} \sum_{\mathsf{f}\in\mathscr{F}_{\mathsf{p}}} \Theta_{\mathsf{f}} \Delta \mathbf{S}_{\mathsf{f}} \,. \tag{24}$$

In order to use this formula, values of the variable at faces are needed. The most straightforward way of obtaining them is using interpolated values from Eq. (12), with shape functions. So we can write

$$(\boldsymbol{\nabla}\Theta)_{\mathsf{p}} \;=\; \frac{1}{\Delta V_{\mathsf{p}}} \sum_{\mathsf{e}\in\mathscr{E}_{\mathsf{p}}} \sum_{\mathsf{f}\in\mathscr{F}_{\mathsf{p}}^{\mathsf{e}}} \sum_{\mathsf{q}\in\mathscr{N}^{\mathsf{e}}} (N_{\mathsf{q}}^{\mathsf{e}})_{\mathsf{f}} \Theta_{\mathsf{q}} \Delta \mathbf{S}_{\mathsf{f}} \,. \tag{25}$$

3.3 Coupling strategy

The coupling strategy chosen to solve the fluid flow and geomechanics is the so-called two-way coupling (Settari and Walters, 2001). It consists in solving the pressure and the displacements linear systems separately, exchanging the information iteratively. Figure 2 illustrates the iterative process by means of a flowchart.

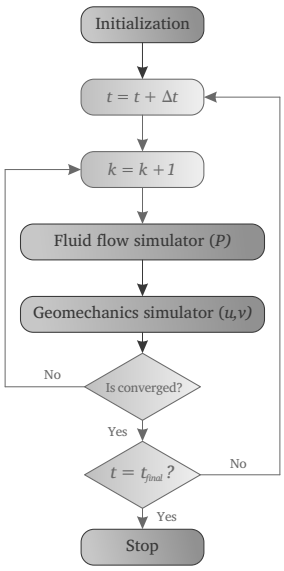

Figure 2. Iterative coupling strategy.

Equation (18) and Eq. (23) are solved in a segregated manner. At each iterative level k, pressure convergence is checked employing the following criterion,

$$\frac{\left\| \mathbf{P}^{k} - \mathbf{P}^{k-1} \right\|_{\infty}}{|P^{k}_{\max} - P^{k}_{\min}|} \leq \tau \,, \tag{26}$$

in which τ is the convergence tolerance. The convergence criterion is based on the infinity norm of the difference between two successive pressure solutions, it means that the coupled solution is reached when there is no significant change on pressure.

4. Numerical results

Two problems with analytical solution are employed to validate the proposed formulation. The first one is the one-dimensional Terzaghi's column and the second one is a two-dimensional problem known as Mandel's problem. These problems will allow us to verify the accuracy of the discretization employed to obtain the coupled solution.

4.1 Terzaghi's column

The Terzaghi's column (Terzaghi, 1923) consists in a fluid-saturated column of height H with a constant loading σ_0 on top, as shown in Fig. 3(a). The lower boundary is fixed while the upper boundary is free to move and allows the

fluid drainage. The load is applied in time t_0, producing a initial solution both for pressure and for vertical displacement, denoted P_0 and v_0. At the same time the upper boundary is open and fluid can leave the domain. The analytical solution for this problem was extracted from Wang (2000) and it considers the y-axis positive downward.

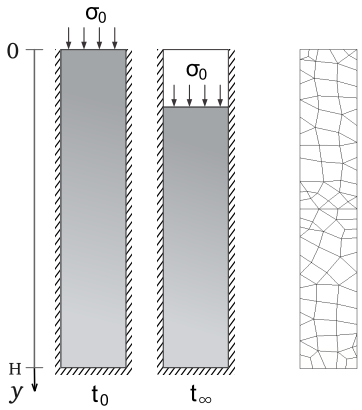

Figure 3. (a) Setup of Terzaghi's consolidation problem and (b) the hybrid grid employed.

For the simulation, it was considered a sandstone homogeneous column with a unit width and height $H = 6$ m. The prescribed top load $\sigma_0 = 10^6$ Pa. The material of the column is a Berea sandstone with the physical properties summarized in Tab. 1, extracted from Wang (2000). The fluid viscosity is $\mu = 0.001$ Pa.s and its compressibility $c_f = 3.030303 \times 10^{-10}$ Pa^{-1}. The hybrid grid used to solve the problem, composed by triangles and quadrangles, is shown in Fig. 3(b). It is formed by 91 elements and 107 nodes, therefore, 107 control volumes can be built on it. A constant time step $\Delta t = 0.1s$ was used for the simulation.

Table 1. Mechanical properties of Berea Sandstone.

Property	**Symbol**	**Value**	**Unit**
Solid grain compressibility	C_s	2.777777×10^{-11}	1/Pa
Biot's coefficient	α	0.777778	-
Porosity	ϕ	0.19	-
Shear modulus	G	6×10^9	Pa
Poisson's coefficient	ν	0.20	-
Undrained Poisson's coefficient	ν_u	0.335034	-
Bulk modulus	K	6×10^9	Pa
Undrained bulk modulus	K_u	1.61855×10^{10}	Pa
Skempton's coeffcient	B	0.650228	Pa
Permeability	$\bar{\mathbf{K}}$	1.9×10^{-15}	m^2

Figure 4(a) corresponds to the pore pressure at the bottom of the column and Fig. 4(b) depicts the vertical displacement at the top of the column. As can be seen in both figures, the numerical solution is very close to the analytical ones showing that the numerical approach presented is accurate solving one-dimensional problems.

4.2 Mandel's problem

Mandel's problem (Mandel, 1953) is a two-dimensional problem that consists in a poroelastic sample, with height $2H$ and length $2L$, sandwiched between two rigid and impermeable plates. A constant and vertical force equal to $2F$ is applied on the outer surfaces of the plates, as shown in Fig. 5(a). The sides are traction-free and allows the fluid draining. Because of the symmetry along both x and y-axis, only a quarter of the domain can be considered for solving this problem.

This problem has also an analytical solution, that can be found in (Abousleiman *et al.*, 1996). Despite the two-dimensional setup of the problem, all variables actually exhibit a one-dimensional behavior. So, for instance, the vertical displacements depend only on y, whereas the others variables depends only on x.

For the time discretization it was used a constant time step $\Delta t = 0.1s$. For the spacial discretization it was considered the grid shown in Fig. 5(b), composed by 57 elements and 71 nodes. The physical properties of the fluid and the porous medium are the same considered in the Terzaghi's problem, presented in the previous section.

Figure 6 shows the behavior of the variables along time. In order to plot these graphs, we chose to plot the time variation of variables at the positions where they have its maximum spatial value. For the pore pressure and the vertical

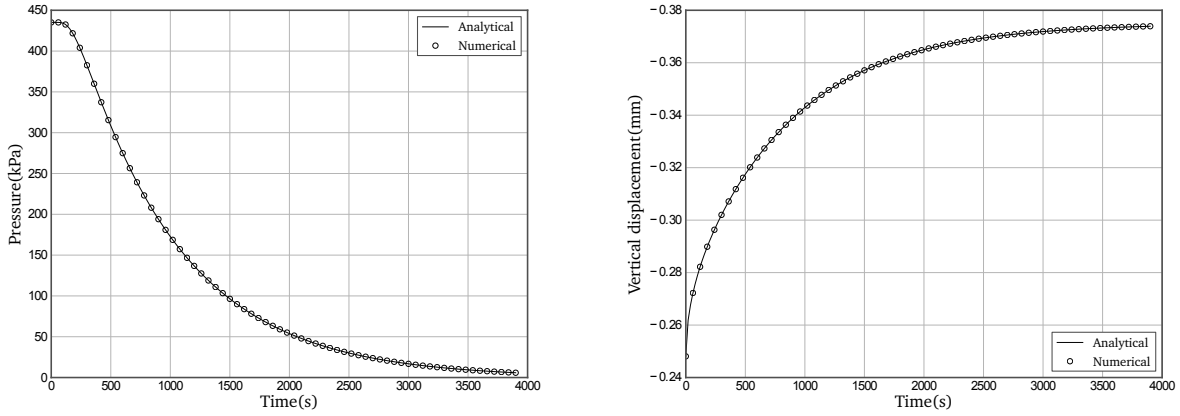

(a) Pore pressure at the bottom of the column along time. (b) Vertical displacement at the top of the column along time.

Figure 4. Terzaghi's Column time results.

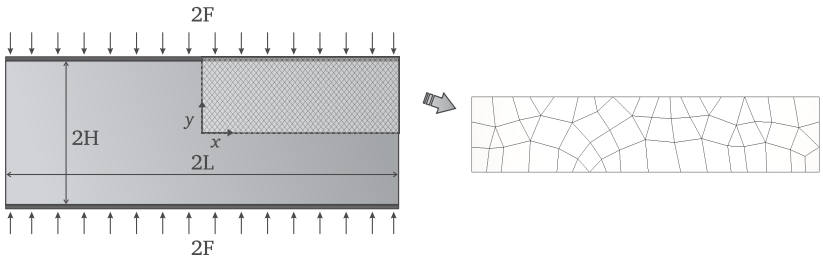

(a) (b)

Figure 5. (a) Setup of Mandel's problem; (b) the hybrid grid employed.

total stress, shown in Fig. 6(a) and Fig. 6(d), respectively, that position is the left boundary. On the other hand, Fig. 6(b) depicts the time variation of the horizontal displacement at the right boundary. Finally, in Fig. 6(c) the vertical displacement at top boundary is plotted along time. As can be seen, the numerical solution shows excellent agreement with the analytical solution, despite the coarseness of the used grid.

5. Conclusion

This work presented a numerical methodology for solving 2D coupled fluid flow and geomechanics in porous media using unstructured grids and finite volume method. This procedure avoids the cumbersome transfer of information from grid to grid when the problem is solved using two different numerical methods, finite element for the rock mechanics and finite volume for the fluid flow. Another feature of the procedure is that the methodology is conservative at discrete level for both physics.

The results show that the methodology, along with two-way coupling strategy, can be very useful to solve coupled problems. It would be necessary a deeper analysis of the methodology, regarding issues like convergence and efficiency, but the first outcome are very promising. Confirmation of the correctness of the numerical solution was made using the analytical solutions of the Terzaghi's column and Mandel's problem.

6. REFERENCES

Abousleiman, Y., Cheng, A.H.D., Cui, L., Detournay, E. and C., R.J., 1996. "Mandel's problem revised". *Géotechnique*, Vol. 46, No. 2, pp. 187–195.

Aziz, K. and Settari, A., 1979. *Petroleum Reservoir Simulation*. Aplied Science Publishers.

Baliga, B.R. and Patankar, S.V., 1980. "A new finite-element formulation for convection-difusion problems". *Numerical Heat Transfer*, Vol. 3, No. 4, pp. 393–409. doi:10.1080/01495728008961767.

Baliga, B.R. and Patankar, S.V., 1983. "A control volume finite-element method for two-dimensional fluid flow and heat transfer". *Numerical Heat Transfer*, Vol. 6, No. 3, pp. 245–261. doi:10.1080/01495728308963086.

Benisch, K., Wang, W., Delfs, J.O. and Bauer, S., 2020. "The ogs-eclipse code for simulation of coupled multiphase flow and geomechanical processes in the subsurface". *Computational Geosciences*, Vol. 24, pp. 1315–1331. doi: 10.1007/s10596-020-09951-8.

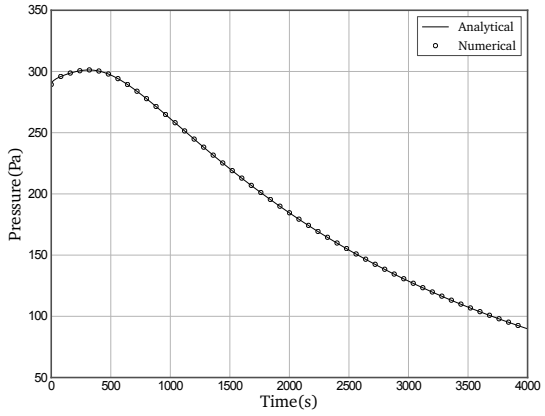

(a) Pressure at the left boundary of the domain along time.

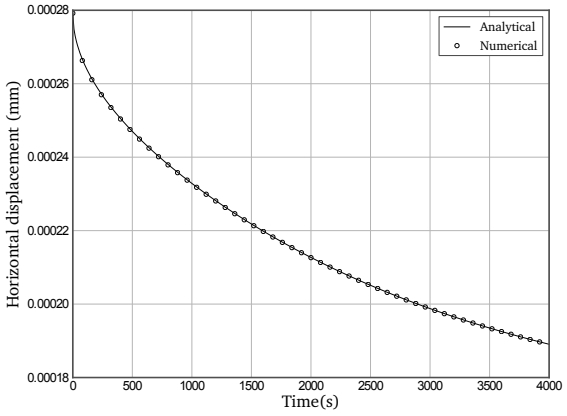

(b) Horizontal displacement at the right boundary of the domain along time.

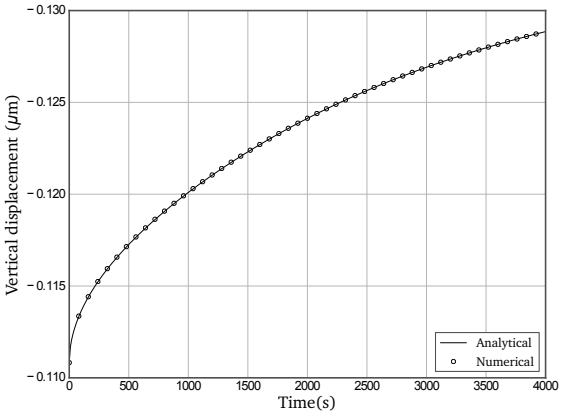

(c) Vertical displacement at the top of the domain along time.

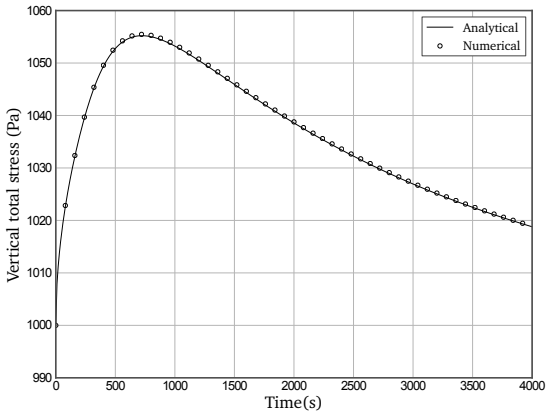

(d) Vertical total stress at the left boundary of the domain along time.

Figure 6. Mandel's problem time results.

Biot, M.A., 1941. "General theory of three-dimensional consolidation". *Journal of Applied Physics*, Vol. 12, No. 2, pp. 155–164. doi:10.1063/1.1712886.

Biot, M.A., 1955. "Theory of elasticity and consolidation for a porous anisotropic solid". *Journal of Applied Physics*, Vol. 26, No. 2, pp. 182–185. doi:10.1063/1.1721956.

Biot, M.A., 1956. "Theory of a porous viscoelastic anisotropic solid". *Journal of Applied Physics*, Vol. 27, pp. 459–167. doi:10.1063/1.1722402.

Blazek, J., 2001. *Computational fluid dynamics: principles and applications*. Elsevier Science Ltd., Oxford, UK.

Chen, Z., Huan, G. and Ma, Y., 2006. *Computational methods for multiphase flows in porous media*. Society for Industrial and Applied Mathematics, Philadelphia, Pennsylvania.

Chin, L., Raghavan, R. and Thomas, L., 2000. "Fully coupled analysis of well responses in stress-sensitive reservoirs". *SPE Reservoir Evaluation & Engineering*, Vol. 3, No. 5, pp. 435–443. doi:10.2118/66222-PA.

Chin, L., Thomas, L., Sylte, J.E. and Person, R.G., 2002. "Iterative coupled analysis of geomechanics and fluid flow for rock compaction in reservoir simulation". *Oil & Gas Science and Technology*, Vol. 57, No. 5, pp. 485–497. doi:10.2118/58968-PA.

Cryer, C.W., 1963. "A comparison of three dimensional consolidation theories of biot and terzaghi". *Quarterly Journal of Mechanics and Applied Mathematics*, Vol. 16, No. 4, pp. 401–412. doi:10.1093/qjmam/16.4.401.

Dal Pizzol, A. and Maliska, C.R., 2012. "A finite volume method for the solution of fluid flows coupled with the mechanical behavior of compacting porous media". *Porous media and Its application in science, Engineering and industry*, Vol. 1453, pp. 205–210.

Detournay, E. and Cheng, A.H.D., 1993. "Fundamentals of poroelasticity". In *Comprehensive Rock Engineering: Principles, Practise and Projects*. Vol. 2, pp. 113–171.

Ferronato, M., Castelletto, N. and Gambolati, G., 2010. "A fully coupled 3-d mixed finite element model of biot consolidation". *Journal of Computational Physics*, Vol. 229, No. 12, pp. 4813–4830. doi:10.2118/87339-PA.

Filippini, G., Maliska, C.R. and Vaz, M., 2014. "A physical perspective of the element-based finite volume method and fem-galerkin methods within the framework of the space of finite elements". *International Journal for Numerical Methods in Engineering*, Vol. 98, pp. 24–43. doi:10.1002/nme.4618.

Forsyth, P.A., 1990. "A control-volume, finite element method for local mesh refinement in thermal reservoir simulation". *SPE Reservoir Engineering*, Vol. 5, No. 4, pp. 561–566.

Geertsma, J., 1966. "Problems of rock mechanics in petroleum production engineering". In *Proceedings of the First Congress of International Society of Rock Mechanics*. Lisboa, Vol. 1, pp. 585–594.

Gottardi, G. and Dall'olio, D., 1992. "A control-volume finite-element model for simulating oil-water reservoirs". *Journal of Petroleum Science and Engineering*, Vol. 8, pp. 29–41.

Gutierrez, M. and Lewis, R.W., 1998. "The role of geomechanics in reservoir simulation". *SPE/ISRM Rock Mechanics in Petroleum Engineering*, , No. 47392, pp. 439–448.

Gutierrez, M. and Lewis, R.W., 2002. "Coupling of fluid flow and deformation in underground formations". *Journal of Engineering Mechanics*, Vol. 128, No. 7, pp. 779–787. doi:10.1061/(ASCE)0733-9399(2002)128:7(779).

Klausen, R.A. and Russel, T.F., 2004. "Relationships among some locally conservative discretization methods which handle discontinuous coefficients". *Computational Geosciences*, Vol. 8, No. 4, pp. 341–377. doi:10.1007/s10596-005-1815-9.

Li, P., Chalaturnyk, R.J. and Tan, T.B., 2006. "Coupled reservoir geomechanical simulations for the sagd process". *Journal of Canadian Petroleum Technology*, Vol. 45, No. 1, pp. 33–40.

Mandel, J., 1953. "Consolidation des sols (Étude mathématique)". *Géotechnique*, Vol. 3, No. 7, pp. 287–299. doi:10.1680/geot.1953.3.7.287.

Mattax, C.C. and Dalton, R.L., 1990. *Reservoir Simulation*, Vol. 13. SPE Monografh Series, Society of Petroleum Engineers.

Mikelič, A., Wang, B. and Wheeler, M.F., 2014. "Numerical convergence study of iterative coupling for coupled flow and geomechanics". *Computational Geosciences*, Vol. 18, No. 3, pp. 287–299. doi:10.1007/s10596-013-9393-8.

Peaceman, D.W., 1977. *Fundamentals of Numerical Reservoir Simulation*. Elsevier Scientific Publishing Company.

Raghavan, R., Scorer, J. and Miller, F., 1972. "An investigation by numerical methods of the effect of pressure-dependent rock and fluid properties on well flow tests". *SPE Journal*, Vol. 12, No. 3, pp. 267–275. doi:10.2118/2617-PA. 2617-PA.

Raw, M., 1985. *A new control-volume based finite element procedure for the numerical solution of the fluid flow and scalar transport equations*. Ph.D. thesis, University of Waterloo, Canada.

Rice, J.R. and Cleary, M.P., 1976. "Some basic stress diffusion solutions for fluid-saturated elastic porous media with compressible constituents". *Reviews of Geophysics and Space Physics*, Vol. 14, No. 2, pp. 227–241.

Rozon, B.J., 1989. "A generalized finite volume discretization method for reservoir simulation". In *SPE Symposion on Reservoir Simulation*. Houston, USA, Paper SPE 18414.

Settari, A. and Walters, D., 2001. "Advances in coupled geomechanical and reservoir modeling with applications to reservoir compactation". *Society of Petroleum Engineers*, pp. 334–342.

Shaw, G. and Stone, T., 2005. "Finite volume methods for coupled stress/fluid flow in a commercial reservoir simulator". *Society of Petroleum Engineers*.

Terzaghi, K., 1923. "Die berechnung der durchlassigkeitsziffer des tones aus dem verlauf der hydrodynamischen spannungsercheinungen". *Sitzungsbere. Akad. Wissen. Wien Math. Naturwis*, Vol. 132, pp. 105–124.

Thomas, L., Chin, L., Pierson, R. and Sylte, J., 2002. "Coupled geomechanics and reservoir simulation". *SPE Annual Technical Conference and Exhibition*. doi:10.2118/77723-MS. 9 pages.

Thomas, L., Chin, L., Pierson, R. and Sylte, J., 2003. "Coupled geomechanics and reservoir simulation". *SPE Journal*, Vol. 8, No. 4, pp. 350–358. doi:10.2118/87339-PA.

Tran, D., Settari, A. and Nghiem, L., 2004. "New iterative coupling between a reservoir simulator and a geomechanics module". *SPE Journal*. doi:10.2118/88989-PA.

Wang, H.F., 2000. *Theory of linear poroelasticity with applications to geomechanics and hydrogeology*. Princeton University Press.

Zienkiewicz, O.C. and Taylor, R.L., 2000. *The finite element method – Volume 1: The basis*. Butterworth-Heinemann, Oxford, England, fifth edition edition.

7. RESPONSIBILITY NOTICE

The authors are solely responsible for the printed material included in this paper.